Volume 10 | Number 23 | 21 June 2019 | Pages 5855–6014

Chemical Science

rsc.li/chemical-science

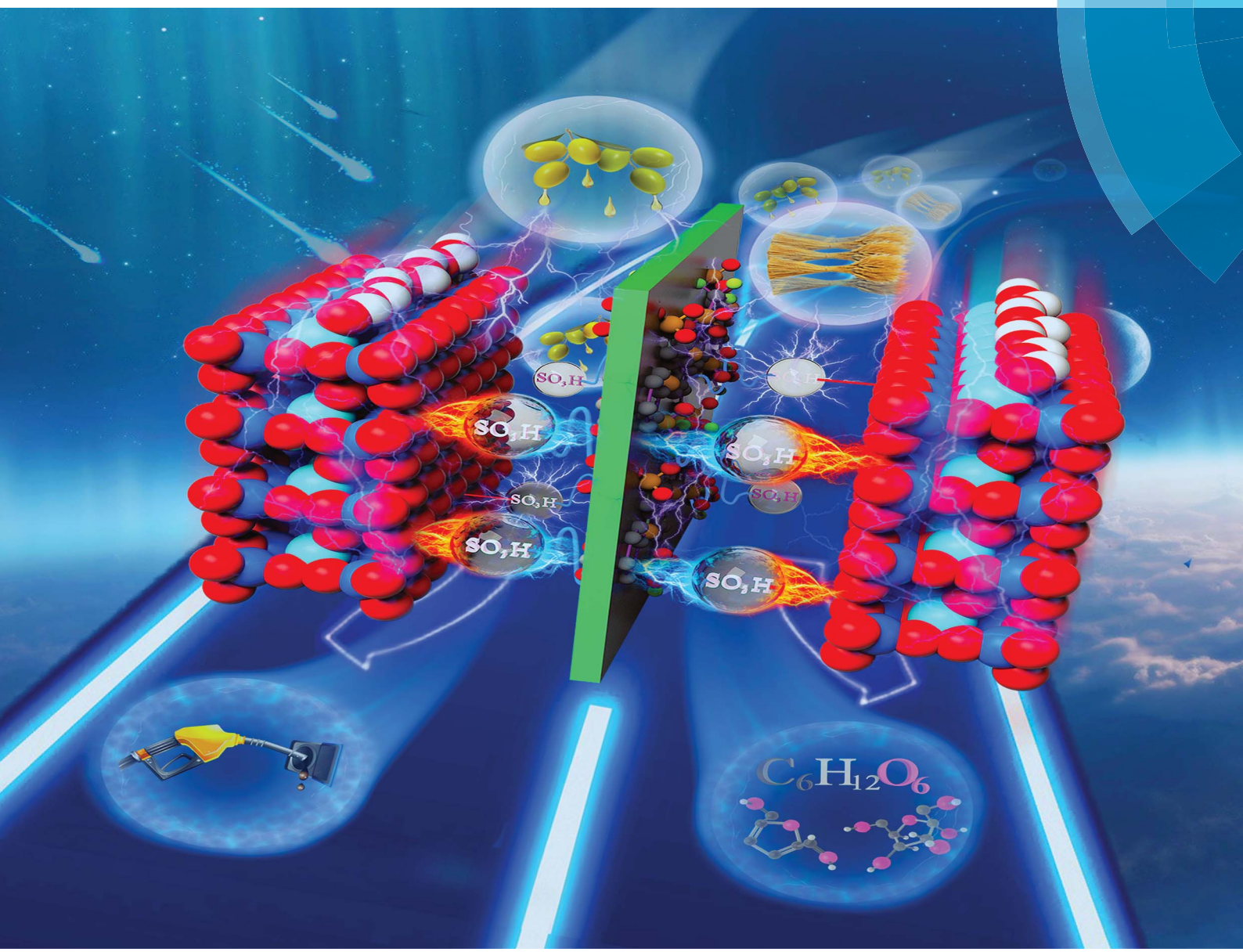

ISSN 2041-6539

ROYAL SOCIETY OF CHEMISTRY | Celebrating IYPT 2019

EDGE ARTICLE

Fujian Liu, Anmin Zheng *et al.*

Developing two-dimensional solid superacids with enhanced mass transport, extremely high acid strength and superior catalytic performance

Chemical Science

EDGE ARTICLE

View Article Online
View Journal | View Issue

Cite this: *Chem. Sci.*, 2019, **10**, 5875

All publication charges for this article have been paid for by the Royal Society of Chemistry

Received 22nd April 2019
Accepted 20th May 2019

DOI: 10.1039/c9sc01988j

rsc.li/chemical-science

Developing two-dimensional solid superacids with enhanced mass transport, extremely high acid strength and superior catalytic performance†

Fujian Liu, *[ab] Xianfeng Yi,[c] Wei Chen, [cd] Zhiqiang Liu,[cd] Wei Chen,[e] Chen-Ze Qi,[a] Yu-Fei Song [e] and Anmin Zheng *[c]

Solid acids have been widely used as heterogeneous catalysts in developing green and sustainable chemistry. However, it remains a challenge to improve the mass transport properties and acid strength of solid acids simultaneously. Herein, we report a class of two dimensional (2D) layered hybrid solid acids with outstanding mass transfer and extremely high acid strength by incorporating sulfonated polymers in-between montmorillonite layers. The 2D layered structure and broad distribution of pore sizes allow for highly efficient mass transport of substrate molecules into and out of the solid acids. The acid strength of these solid acids was found to be stronger than that of 100% H_2SO_4, $H_3PW_{12}O_{40}$ and any other reported solid acids to date, as determined by ^1H and ^{31}P solid-state NMR. These 2D solid acids show extraordinary catalytic performance in biomass conversion to fuels, superior to that of $H_3PW_{12}O_{40}$, HCl and H_2SO_4. Theoretical calculations and control experiments reveal that H-bond based interactions between the polymer and montmorillonite facilitate the unusually high acid strengths found in these samples.

Introduction

Solid acids are one of the most important catalysts used in industry.[1–4] Compared to liquid acids, solid acids cause less corrosion of the facility,[5–9] can be easily separated from the reaction medium for recycling,[10–14] and their properties may be tunable for specific feedstock and products.[15–19] However, widely used solid acids such as natural clays, sulfated metal oxides, and ion-exchange resins have poor porosity that limits the exposure of their acidic sites to the substrate molecules.[2,7,14,20] Solid acids such as zeolites and sulfonated mesoporous materials have abundant, nanometer-scaled pores, which considerably enhance the accessibility of acidic sites to the substrate molecules during reactions.[3,21–23] However, the three dimensional, connected network of the pores may give rise to locally confined spaces and limit the diffusion of large molecules or macromolecules into and out of the system.[24,25] In addition to improving the accessibility of acidic sites and enhancing mass transport, it is also desirable to incorporate the strongest possible acid centers into solid acids,[10,11,22,24] to lower the activation energy in acid-catalyzed reactions. Integrating all these designing factors into the molecular engineering of solid acids, however, remains challenging in the field.

The emergence of two dimensional (2D) materials provides a new opportunity in designing new solid acids to overcome this challenge.[25–31] When organized as layered structures, 2D materials such as graphene and its derivatives usually facilitate enhanced mass transfer of guest molecules and can be chemically modified to incorporate specific acid groups. The enhanced mass transfer can be attributed to the improved wettability and unique nanosheet structures in these 2D materials.[25,26] However, it is usually difficult to graft abundant acidic sites onto the surface of graphene and its derived materials, due to the inert nature of the sp^2 carbon.[25,26] In addition, the regeneration of graphene-based materials is challenging as they are not readily separated from the reaction mixture.[25,26] Although some early studies, *e.g.*, based on sulfated graphene, showed promising results, none of these studies have yet succeeded in controlling wettability, improving mass transportation and enhancing acidity simultaneously.[25–29]

In general, the acid strength of solid acids could be enhanced by introducing strong electron-withdrawing moieties

[a]*Key Laboratory of Alternative Technologies for Fine Chemicals Process of Zhejiang Province, College of Chemistry and Chemical Engineering, Shaoxing University, Shaoxing, 312000, China*

[b]*National Engineering Research Centre of Chemical Fertilizer Catalyst (NERC-CFC), School of Chemical Engineering, Fuzhou University, Fuzhou, 350002, China. E-mail: fjliu@fzu.edu.cn*

[c]*Wuhan Center for Magnetic Resonance, Key Laboratory of Magnetic Resonance in Biological Systems, State Key Laboratory of Magnetic Resonance and Atomic and Molecular Physics, Wuhan Institute of Physics and Mathematics, Chinese Academy of Sciences, Wuhan 430071, China. E-mail: zhenganm@wipm.ac.cn*

[d]*University of Chinese Academy of Sciences, Beijing 100049, China*

[e]*State Key Laboratory of Chemical Resource Engineering, Beijing University of Chemical Technology, 100029 Beijing, China*

† Electronic supplementary information (ESI) available: detailed descriptions of the apparatus and synthetic methods, 29 figures, and 5 tables. See DOI: 10.1039/c9sc01988j.

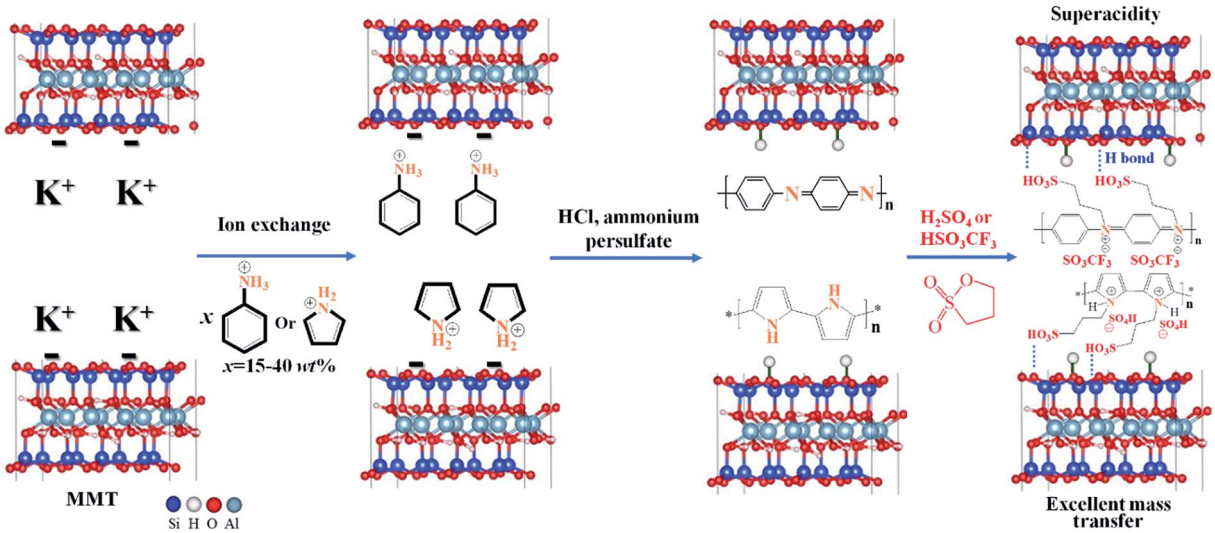

Scheme 1 Synthetic route for 2D hybrid solid superacids MMT@PAN-[C_3N][SO_3CF_3] and MMT@PPY-[C_3N][SO_4H].

(*e.g.*, fluorine containing groups) on their surface.[2,23] In particular, grafting fluorine-containing groups onto solid acids is a good choice, due to the improved stability.[6,22] A variety of polymeric acids have also been incorporated into 3D silica materials, which exhibit enhanced acidity due to the confinement effect.[10,24,32–36] Alternatively, taking advantage of the confinement effect in layered 2D materials and molecular engineering of the local electronic environment may provide new routes to 2D solid acids with a desired acid strength and surface wettability. Herein, we design a class of hybrid solid superacids based on a 2D montmorillonite (MMT) scaffold by polymerizing nitrogen-containing monomers such as aniline and pyrrole in-between the MMT layers (Scheme 1). The polymers are sulfonated subsequently to facilitate extremely high acidity, because of the unique hydrogen bonding between the MMT and sulfonic groups in polymer species. Their acid strength was stronger than that of 100% H_2SO_4, phosphotungstic acid and any other reported solid acids to date. The interstices in-between the MMT layers are 2D in nature and vary in the domain sizes. After aniline and pyrrole molecules are intercalated into the interstices and polymerized, the resultant polymers can be further functionalized to include superacidic sites and to possess good wettability. We found that both small organic molecules and large macromolecules can have efficient mass transport into and out of the 2D solid superacids. The synergistic effect of good wettability, record-high acid strength, and efficient mass transportation thus gives rise to an extraordinary catalytic performance in the degradation of cellulose, a major component of biomass and, a class of macromolecules that are usually very difficult to deal with by using solid acids.

Results and discussion

Our proposal is to incorporate sulfonated polymers in-between MMT layers and find the conditions under which the resulting materials may simultaneously possess good wettability, super acidity, and excellent mass transporting properties. The procedure for the synthesis of the 2D hybrid solid acid is illustrated in Scheme 1. We first use ion exchange to replace K^+ with protonated aniline in the interlayer of MMT. The intercalated aniline was then self-polymerized in-between the MMT layers to give a MMT@PAN composite, and then the released H^+ combines with O^- anchored onto the network of MMT, which results in the formation of a hydroxyl group. MMT@PAN was further sulfonated with 1,3-propanesultone and ion exchanged with trifluoromethanesulfonic acid or sulfuric acid to give 2D hybrid solid acids MMT@PAN-[C_3N][SO_3CF_3] and MMT@PAN-[C_3N][SO_4H]. Besides aniline, protonated pyrrole can also be used as the monomers and polymerized in-between MMT to obtain MMT@PPY, and $[SO_4H]^-$ can be incorporated as the anion in this system (Scheme 1). Altogether, three different samples, MMT@PAN-[C_3N][SO_3CF_3], MMT@PAN-[C_3N][SO_4H] and MMT@PPY-[C_3N][SO_4H] were prepared. We control the extent of sulfonation of the polymers in MMT to tune the surface wettability and porosity of the samples. The morphology and structures of the hybrid solid acids are shown in Fig. S1.† All the samples exhibit periodic 2D layered structures.

Fig. S2† shows N_2 isotherms and the pore size distribution of the synthesized samples. MMT shows a type II isotherm with 2D layered characteristics,[37] showing an upsurge at a relative pressure (P/P_0) between 0.5 and 1.0. After intercalation of polymers into MMT (*e.g.*, MMT@PAN and MMT@PPY) and subsequent sulfonation, the resultant 2D solid acids exhibit similar isotherms with 2D layered characteristics, but reduced volume of adsorption resulting from the incorporation of polymers into the interstices. In comparison, MMT has a BET surface area of 101 $m^2\ g^{-1}$, while MMT@PAN, MMT@PPY, and the obtained 2D solid acids all show reduced BET surface areas ranging from 29 to 97 $m^2\ g^{-1}$ (Table S1†). Besides, the hierarchical structures in these samples possess a wide size distribution ranging from 2.3 to 129.2 nm (Fig. S2†).

The successful grafting of sulfonic group onto the 2D hybrid solid acids was confirmed by XPS and FT-IR spectroscopy. Except for MMT, additional signals of S_{2p}, C_{1s}, N_{1s}, O_{1s} and F_{1s} could also be observed in these samples (Fig. S3†). The signals of S_{2p} at around 168–170 eV were assigned to the sulfonate group, $[SO_4H]^-$ and $[SO_3CF_3]^-$ anions. The signals of C_{1s} were fitted and deconvoluted into several peaks centered at around 284.5, 286.6, 289.7 and 292.3 eV, corresponding to the C–C, C–N, C–S and C–F bonds, respectively.[22] The signals of N_{1s} were fitted and deconvoluted into two peaks, assigned to aniline or pyrrole N, and quaternized N with 1,3-propanesultone. FT-IR spectra also confirm the successful incorporation of sulfonic groups into PAN and PPY (Fig. S4†). The additional broad peaks at around 1040, 1086 and 1186 cm^{-1} were assigned to C–S and S=O bonds,[22] in good agreement with XPS results. The sulphur contents of the 2D solid acids were measured to be from 1.24 to 1.36 mmol g^{-1}, and their H^+ ion capacities range from 1.32–1.83 mmol g^{-1} (Table S1†), lower than that of Amberlyst-15, but higher than that of Nafion NR50. The above results indicate that the hybrid solid acids have well-defined structures with adjustable concentrations of acid groups.

The structures of the synthesized 2D hybrid solid acids are characterized by X-ray diffraction (XRD) and high-resolution transmission electron microscopy (HR-TEM). A well-defined layered structure could be detected before and after the introduction of sulfonated polymers into MMT. Fig. S5† shows the XRD patterns of MMT, MMT@PAN, MMT@PPY and the three 2D solid acids samples: MMT@PPY-$[C_3N][SO_4H]$, MMT@PAN-$[C_3N][SO_4H]$ and MMT@PAN-$[C_3N][SO_3CF_3]$. Compared with pristine MMT, the α peaks associated with (001) diffraction became wider for MMT@PPY-$[C_3N][SO_4H]$, MMT@PAN-$[C_3N][SO_4H]$ and MMT@PAN-$[C_3N][SO_3CF_3]$, and the peak positions shifted from 5.77 to 6.67°. This change indicates that the average layer distance of MMT decreases from 1.54 to 1.33 nm after introducing the sulfonated polymers. In general, the intercalation of polymer additives into the interlayer of MMT usually results in the extension of its interlayer distance. The nearly 14.4% shrinkage of the layer distance should come from the strong interactions between sulfonated polymers and the MMT support. Interestingly, after calcination of MMT@PAN-$[C_3N][SO_3CF_3]$ with oxygen to remove the sulfonated polymer, the residual MMT support shows a similar pattern to pristine MMT. This phenomenon further confirms the successful intercalation of the sulfonated polymer into the interlayer of MMT and the strong interactions between the sulfonated polymer and MMT layers. The successful intercalation of the sulfonated polymer into the interlayer of MMT can be further confirmed by fabricating an inverted structure of MMT, in which sulfonated polymer wrapped MMT (designated as MMT-PAN-$[C_3N][SO_3CF_3]$) was prepared for comparison. Both MMT@PAN-$[C_3N][SO_3CF_3]$ and MMT-PAN-$[C_3N][SO_3CF_3]$ were carbonized and etched with HF for the removal of the MMT scaffold. The resultant MMT@carbon shows a much enhanced porosity in comparison with MMT-carbon (Fig. S6†). The incorporation of the polymers into MMT increases the heterogeneity of the system and leads to the decreased crystallinity of MMT (broadening of the α peak), which results in the formation of structural defects and locally distorted structures with different domain sizes in the samples. The mentioned hierarchical structures may provide the opportunity for guest molecules of different sizes to diffuse into and out of the solid acids and afford diverse local environments for acid catalyzed reactions. Similar hierarchically layered structures with abundant and different domain sizes (Fig. S7†) were observed by scanning electron microscopy (SEM). The HR-TEM images and STEM images of the synthesized 2D solid acids are shown in Fig. 1, in which highly ordered, periodic layer-by-layer structures coexist with locally distorted structures with different domain sizes in these samples. The hybrid layered structures were also confirmed by elemental linear scanning (Fig. S8†). The elemental maps of MMT@PAN-$[C_3N][SO_4H]$ in Fig. S8† indicate the relatively homogeneous distribution of Si, Al, C, N, O and S in the crystalline domains of the samples, consistent with XPS and FT-IR spectra.

We firstly compared the diffusion properties of the 2D hybrid solid acids with those of 3D mesoporous solid acids of SBA-15-SO_3H-0.2, commercial Amberlyst-15 and superacid of Nafion NR50 in the esterification of acetic acid with cyclohexanol. As shown in Fig. 2, the catalytic efficiencies of SBA-15-SO_3H-0.2, Amberlyst-15 and Nafion NR50 in the reaction depend on the stirring rates, indicating that the process is limited by diffusion of molecules into the inner pores of solid acids. In contrast, the catalytic efficiencies of the 2D solid acids are almost independent of the stirring rate, and can reach very high levels even without stirring. This phenomenon used to only exist in strong liquid acids such as H_2SO_4 (Fig. 2). The result indicates the outstanding mass transporting properties of 2D hybrid solid acids. In addition, the 2D hybrid solid acids have much higher TOF values and better activities than H_2SO_4, Nafion NR50 and Amberlyst-15 under the same reaction conditions (Table S2†).

To understand the molecular basis of the mass transport properties, we used theoretical calculations to compare the mass transport properties of 2D MMT with those of 3D connected zeolites such as MFI, MOR and VFI. The mass transport properties of different solid acids were studied by molecular dynamics (MD) (Fig. S9 and S10†). We found that the diffusion of small molecules such as methanol or acetic acid in MMT was at least 1 order faster than that in zeolites with 3D micropores (Table S3†). Presumably, the unique 2D layered structures, together with a controllable and good surface wettability (Fig. S11†), promote the mass transportation of molecules into and out of the MMT support.

In addition to mass transport, the acid strength plays a critical role in the catalytic performance of solid acids. We found that the acid strength of the 2D solid acids was effectively enhanced *via* the molecular interactions between the sulfonated polymer and MMT in close proximity. The acidity of the synthesized 2D solid acids was investigated by using ^1H and ^{31}P MAS NMR, a reliable and state-of-the-art technique for determination of the acidity of solid acid catalysts.[6,9,24,38,39] In particular, ^{31}P trialkylphosphine (TMP) NMR has been used to distinguish Brønsted and/or Lewis acid types. When TMP molecules are bound to Lewis acid sites, they give rise to ^{31}P resonance ranging from *ca.* −20 to −60 ppm. In contrast,

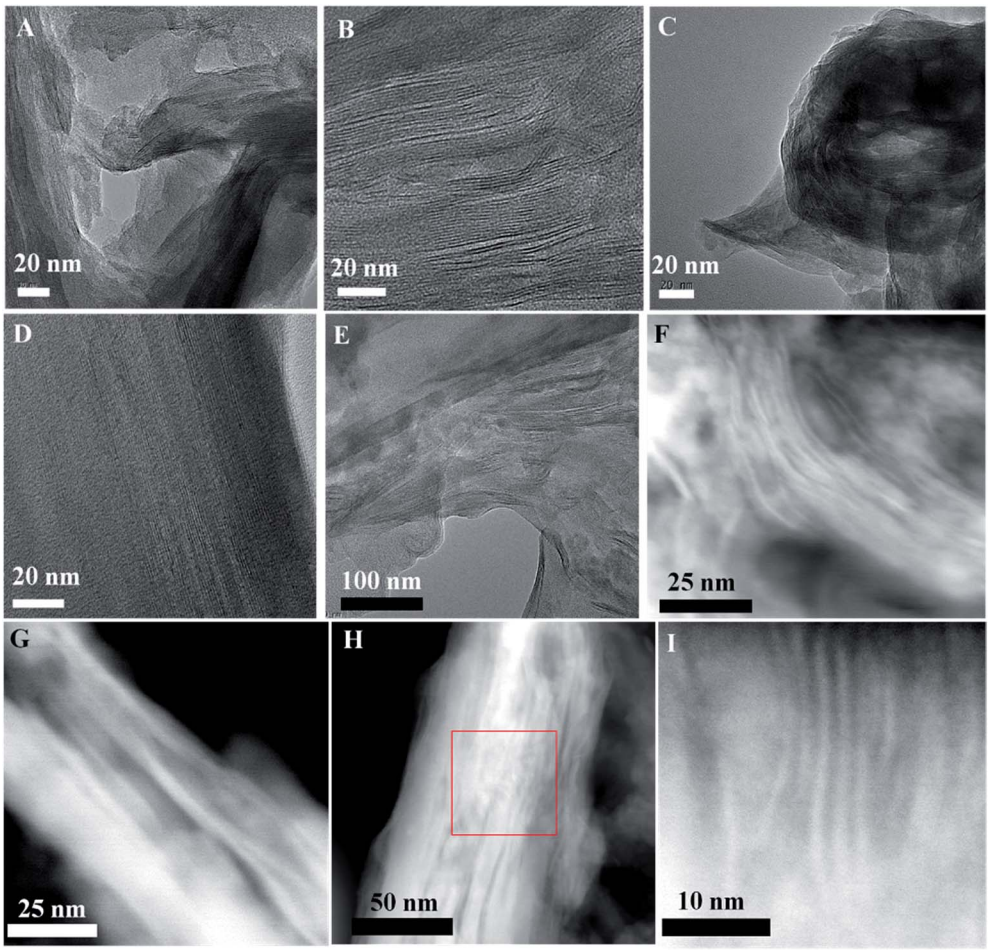

Fig. 1 HR-TEM images of (A and B) MMT@PPY-[C_3N][SO_3CF_3], (C and D) MMT@PAN-[C_3N][SO_4H], and (E) MMT@PAN-[C_3N][SO_3CF_3], and STEM images of (F) MMT@PAN-[C_3N][SO_4H], (G) MMT@PPY-[C_3N][SO_3CF_3] and (H and I) MMT@PAN-[C_3N][SO_3CF_3].

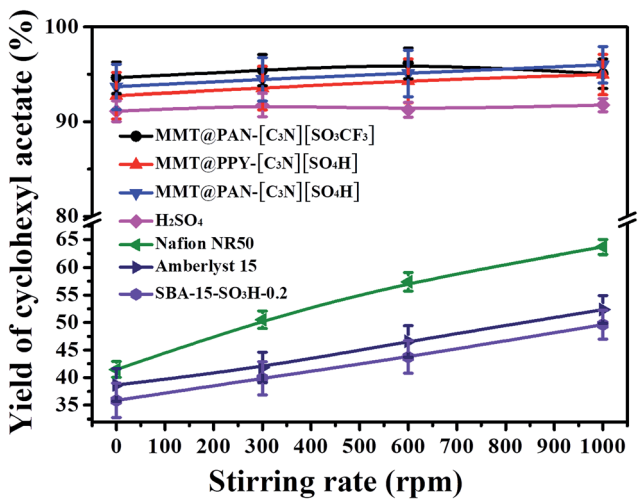

Fig. 2 The yields of cyclohexyl acetate in the esterification of acetic acid with cyclohexanol catalyzed by various solid acids at different stirring rates (0.11 mol of cyclohexanol, 0.305 mol of acetic acid, 0.15 g of solid acids, 100 °C for 5 h; H_2SO_4: the same number of H^+ sites as MMT@PAN-[C_3N][SO_3CF_3]).

$TMPH^+$ ions, which are protonated by the Brønsted acidic proton, normally lead to ^{31}P resonances at *ca.* −2 to −5 ppm.[6,9,24,38,39] We found that ^{31}P NMR only resides at −2.9 ppm for TMP adsorbed on MMT@PAN-[C_3N][SO_3CF_3], suggesting a Brønsted acid (Fig. S12a†).[6,9,40] In general, both Lewis and Brønsted acid sites are expected to exist in MMT due to the presence of Al^{3+} ions in low coordination.[41,42] This assessment was confirmed by ^{31}P TMP NMR; the Lewis acid site in MMT shows a broad and weak signal (Fig. S12b†). However, no signal of the Lewis acid site was detected in MMT@PAN-[C_3N][SO_3CF_3], likely due to the loss of most Lewis acid sites during the preparation process involving the treatment with a strong acid (HSO_3CF_3).[41,42]

The acid strength of MMT@PAN-[C_3N][SO_3CF_3] was determined by using ^{31}P trimethylphosphine oxide (TMPO) NMR, where a larger ^{31}P chemical shift of adsorbed TMPO indicates stronger acidity. As shown in Fig. 3, the MMT support displayed two distinct ^{31}P resonances at $\delta^{31}P$ of 46 and 55 ppm, which are assigned to the physisorbed TMPO and TMPO adsorbed on weaker acidic sites, respectively. MMT possesses sites with weaker acidity comparable to those of HY zeolites (55–65 ppm).[6,41] Meanwhile, the sulfonated polymer of PAN-[C_3N]

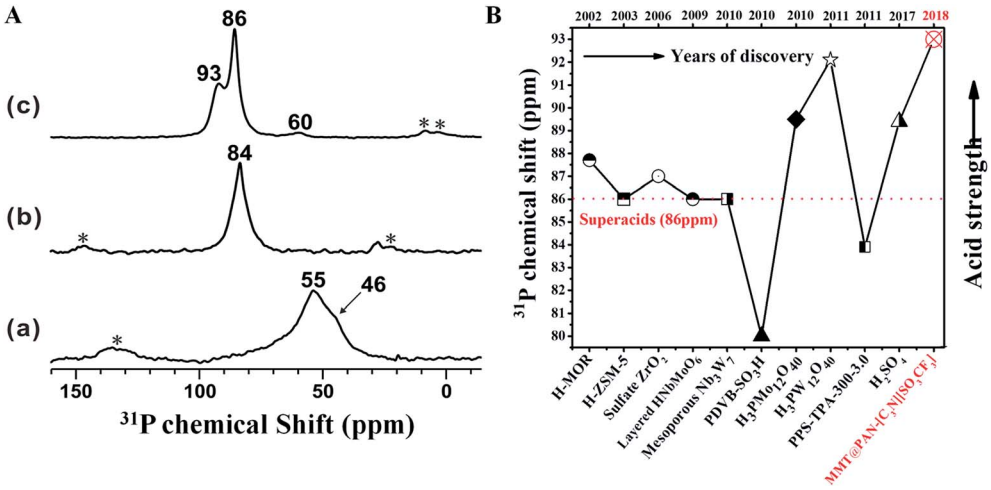

Fig. 3 (A) Room temperature ^{31}P MAS NMR spectra of trimethylphosphine oxide (TMPO) adsorbed on (a) MMT support, (b) PAN-$[C_3N][SO_3CF_3]$ and (c) MMT@PAN-$[C_3N][SO_3CF_3]$; (B) the comparison of the acid strength of MMT@PAN-$[C_3N][SO_3CF_3]$ with that of various reported acids.[6]

$[SO_3CF_3]$ showed enhanced acidity, giving ^{31}P spectra with TMPO adsorption at 84 ppm. The intercalation of the sulfonated polymer into the MMT layer results in a significant increase of the acid strength with ^{31}P chemical shifts found at 86 and 93 ppm (Fig. 3A and S13†), corresponding to two types of superacid sites formed in MMT@PAN-$[C_3N][SO_3CF_3]$, which should be attributed to the sulfonated polymer intercalated in both locally distorted structures and the interlayer of MMT. A chemical shift above 86 ppm in ^{31}P TMPO NMR was commonly used to identify superacids.[6] As far as we know, the measured δ^{31}P value of 93 ppm is by far the largest chemical shift reported for TMPO adsorbed on solid acids (Fig. 3B).[6] Therefore, the acid strength of the 2D solid acid is stronger than any other reported solid acids to date, which is even higher than that of 100% H_2SO_4 and $H_3PW_{12}O_{40}$, both of which have a ^{31}P chemical shift at nearly 89.4 and 92.1 ppm.[6,43,44] The unusually high acid strength of MMT@PAN-$[C_3N][SO_3CF_3]$ has been further confirmed by the Hammett indicator method.[11] The UV spectra of the solutions with the indicator (4-nitrofluorobenzene) were collected, showing a much stronger adsorption peak for MMT@PAN-$[C_3N][SO_3CF_3]$ than for H_2SO_4 (Fig. S14†). The result confirms that the acidity of MMT@PAN-$[C_3N][SO_3CF_3]$ ($H_0 < -12.4$) is stronger than that of H_2SO_4. Furthermore, potentiometric titration was used to characterize the acidity of MMT@PAN-$[C_3N][SO_3CF_3]$; the very high initial electric potential (617.8 mV) of MMT@PAN-$[C_3N][SO_3CF_3]$ further confirms its superacidity (Fig. S15†),[45] in good agreement with ^{31}P solid state NMR. Likely, the superacidity of the 2D hybrid solid acids is a result of the interactions between the sulfonated polymer and the MMT scaffold, which promotes the release of H^+ in the sulfonate group.

The enhanced mass transfer and superacidity facilitate the excellent catalytic efficiency of 2D solid acids, and their catalytic performance was evaluated in important acid-catalyzed reactions of biomass conversion to fuels, which include towards transesterification to biodiesel and depolymerization of crystalline cellulose to sugars and fine chemicals. Fig. 4 and S16† show the kinetic curves and calculated activation energy in the transesterification of tripalmitin with methanol over various catalysts, where methyl palmitate was the only product. The 2D solid acids showed far better catalytic activities than Amberlyst-15, SBA-15-SO_3H-0.2, Nafion NR50, porous SO_4/ZrO_2 and $H_3PW_{12}O_{40}$, as well as H_2SO_4. The acid strength of the solid acids was found to be correlated with the activation energy of the reaction. For instance, MMT@PAN-$[C_3N][SO_3CF_3]$ shows an activation energy of 34.32 kJ mol^{-1}, much lower than those of H_2SO_4 (45.84 kJ mol^{-1}), $H_3PW_{12}O_{40}$ (50.05 kJ mol^{-1}), Nafion NR50 (59.74 kJ mol^{-1}), Amberlyst-15 (88.36 kJ mol^{-1}) and SBA-15-SO_3H-0.2 (95.55 kJ mol^{-1}) under experimental conditions. The acid strength (evaluated from ^{31}P chemical shifts) and activation energy in this reaction show a strong correlation (Fig. S17†), suggesting that the acid strength is regulated by the activation energy of solid acid catalysts. Combining the ultra-strong acid strength and outstanding mass transport properties, much higher TOF values and initial reaction rates were found in MMT@PAN-$[C_3N][SO_3CF_3]$ than H_2SO_4, Amberlyst-15 and Nafion NR50 (Table S2 and S4†).

The 2D solid acids also showed impressive activities for the conversion of low quality plant oil to biodiesel (Table S5†), in which eight methyl ester products with varying lengths of the carbon chain and unsaturated levels were detected. The yields of biodiesel reach 94.2–99.1% in the reactions catalyzed by the 2D solid acids, far better than those of $H_3PW_{12}O_{40}$ (69.8–74.1%), PAN-$[C_3N][SO_4H]$ (86.5–89.2%), porous SO_4/ZrO_2 (29.3–40.9%), SBA-15-SO_3H-0.2 (33.5–58.2%), Amberlyst-15 (29.8–51.7%) and H-USY (9.3–20.6%). Once again, the activities of the synthesized 2D solid acids are better than those of strong liquid acids such as H_2SO_4 (95.9–98.1%). Unlike liquid acids, these 2D solid acids could be easily recovered by centrifugation. Their activities largely remained the same even after five times of recycling. The excellent reusability of the 2D solid acids should be due to their superior mass transfer and enhanced hydrothermal stabilities; the sulfonic groups in the 2D solid acids only start to decompose at a temperature above 250 °C under ambient conditions

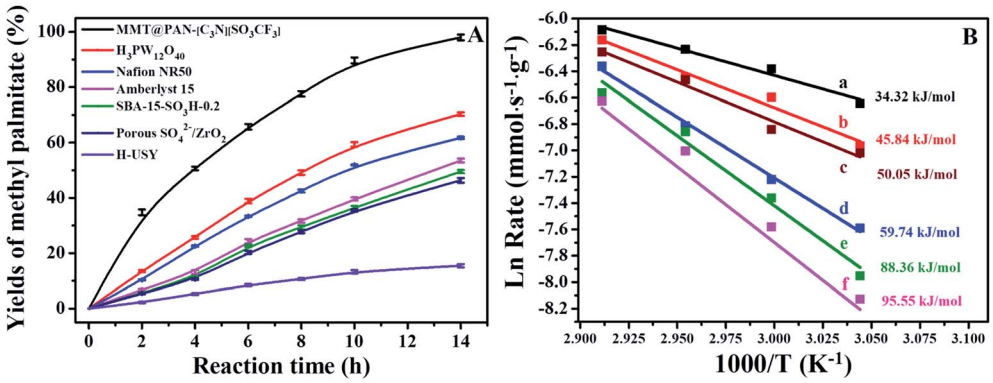

Fig. 4 (A) The yields of methyl palmitate catalyzed by various acid catalysts, and (B) activation energies (E_a) of (a) MMT@PAN-$[C_3N][SO_3CF_3]$, (b) H_2SO_4, (c) $H_3PW_{12}O_{40}$, (d) Nafion NR50, (e) Amberlyst-15 and (f) SBA-15-SO_3H-0.2 in the transesterification of tripalmitin with methanol.

Table 1 Yields of dehydration products in the depolymerization of Avicel catalyzed by various solid acids

Catalysts	Glucose yield[a] (%)	Cellobiose yield[a] (%)	Cellobiose yield[b] (%)	TRS[c] (%)
Amberlyst-15	27.5	19.1	3.9	56.2
$H_3PW_{12}O_{40}$	37.2	18.5	4.6	68.7
SBA-15-SO_3H-0.2	22.7	13.8	4.5	47.2
HCl	66.5	13.7	9.3	94.8
PAN-$[C_3N][SO_3CF_3]$	55.5	11.6	7.9	83.4
MMT@PAN-$[C_3N][SO_3CF_3]$	79.5	9.1	8.5	99.5
MMT@PAN-$[C_3N][SO_4H]$	77.6	8.9	7.7	98.2
MMT@PPY-$[C_3N][SO_4H]$	76.9	9.4	6.3	96.3

[a] Measured by the HPLC method; the reaction was performed at 100 °C for 5 h. [b] Yields of HMF were measured by GC-MAS. [c] Yields of TRS were measured by the DNS method.

(Fig. S18 and 19†), while the polymer networks start to decompose at a temperature above 450 °C due to their large molecular weights (M_w of PAN-$[C_3N][SO_3CF_3]$ and PPY-$[C_3N][SO_4H]$ was measured to be ~22k and ~23k g mol^{-1}, respectively, Fig. S20†) and strong interactions with the MMT scaffold, which can prevent the decomposition of the sulfonated polymer in a low temperature range (<250 °C).

To further demonstrate the capability of the 2D solid acids, we investigate their catalytic efficiency in the depolymerization of crystalline cellulose (Avicel), which is usually very difficult to deal with using traditional solid acids. When the reaction is catalyzed by MMT@PAN-$[C_3N][SO_3CF_3]$, the total reducing sugar was up to 99.5%, with the yields of glucose, cellobiose and HMF measured to be 79.5, 9.1 and 8.5%, respectively. High catalytic efficiencies could also be found in MMT@PAN-$[C_3N][SO_4H]$ and MMT@PPY-$[C_3N][SO_4H]$. The yields of glucose, cellobiose and HMF reach ~77%, ~9%, and ~7% within 5 h of reaction, and the total reducing sugar was almost ~98%. The catalytic activities of the 2D solid acids were much higher than those of Amberlyst-15, $H_3PW_{12}O_{40}$ and SBA-15-SO_3H-0.2, as well as HCl and PAN-$[C_3N][SO_3CF_3]$ (Table 1). The superior catalytic activities of the 2D solid acids should be attributed to their extremely high acid strength and the presence of hierarchically 2D distorted structures, which can be verified by the adsorption of Avicel. The mentioned hierarchically 2D nanostructures were large enough for the Avicel macromolecules to diffuse into and out of the sample (Fig. S21†), and thereby facilitate fast deconstruction of Avicel in the reaction (Fig. S22†).

To understand the unusual acid strength of the synthesized 2D solid superacids, ^{1}H solid state NMR was used to investigate the behavior of –SO_3H in MMT@PAN-$[C_3N][SO_3CF_3]$. As shown in Fig. 5, the ^{1}H peak at 4.4 ppm was assigned to the acidic proton in –SO_3H.[46] The ^{1}H peaks at 6.7–8.0 ppm were assigned to hydrogen atoms in the –NH_2– group, and the peaks at 0.8–2.5 ppm were attributed to the –CH_2– group bound to –SO_3H. In contrast to PAN-$[C_3N][SO_3CF_3]$, the intensities of peaks at *ca.* 6.7–8.0 ppm were enhanced (Fig. 5b), and a new lower-field peak at 16.7 ppm appeared in MMT@PAN-$[C_3N][SO_3CF_3]$. We believe that this is due to the confinement effect of 2D layered MMT, which allows for the formation of strong H-bonds between intercalated PAN-$[C_3N][SO_3CF_3]$ and MMT, further enhancing the acid strength. It is noteworthy that –SO_3H in MMT@PAN-$[C_3N][SO_3CF_3]$ cannot fully interact with the MMT scaffold because of the intrinsic steric hindrance effect, which results in the presence of a lower chemical shift of TMPO at around 86

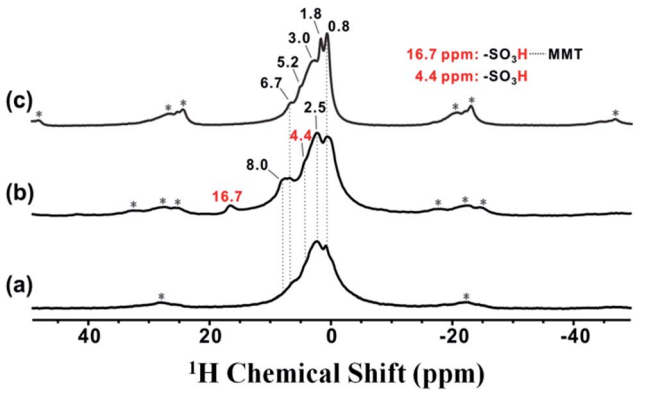

Fig. 5 ^{1}H solid-state NMR spectra of (a) PAN-$[C_3N][SO_3CF_3]$, (b) MMT@PAN-$[C_3N][SO_3CF_3]$ and (c) trifluoroacetic acid treated MMT@PAN-$[C_3N][SO_3CF_3]$. The asterisks in the ^{31}P NMR spectra denote spinning sidebands.

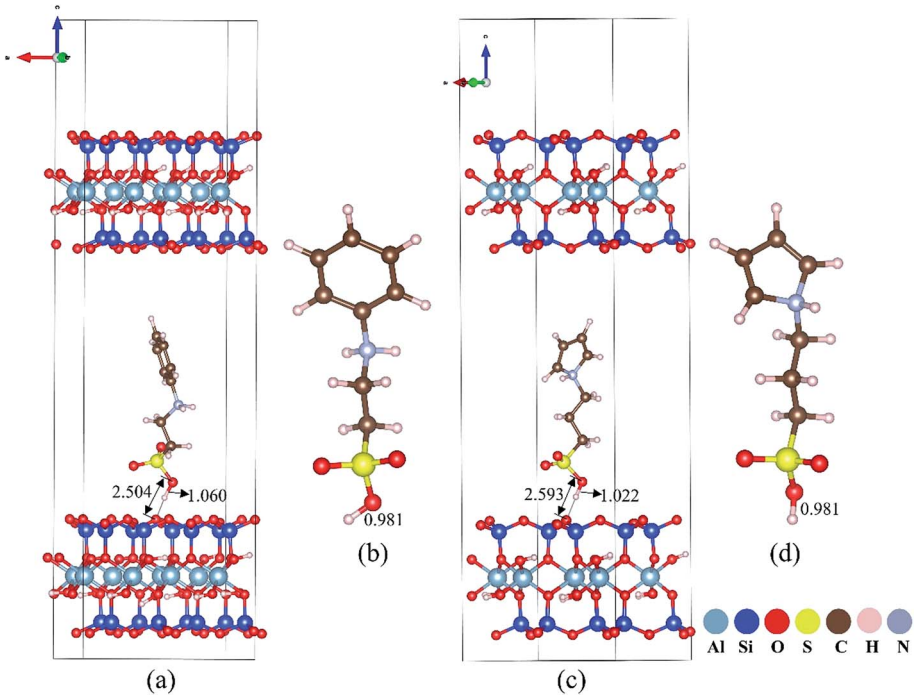

Fig. 6 The optimized structural parameters of sulfonated aniline and pyrrole in MMT (a and c) and sulfonated aniline and pyrrole monomers (b and d). The calculated O–H interatomic distances (in Å) are indicated.

ppm (as depicted in Fig. 3A). To further confirm the intermolecular hydrogen bonding interaction, MMT@PAN-[C_3N][SO_3CF_3] was treated with trifluoroacetic acid, an acid commonly used to interrupt H-bond interactions in molecules.[47] We found, after treating MMT@PAN-[C_3N][SO_3CF_3] with trifluoroacetic acid, that the intensities of peaks at *ca.* 6.7–8.0 ppm decreased, and the lower-field peak at 16.7 ppm disappeared. This result confirms the existence of H-bonds between intercalated PAN-[C_3N][SO_3CF_3] and MMT.

The molecular nature of H-bond interactions between sulfonated polymers and MMT was further investigated by using DFT calculations. The length of the O–H bond in –SO_3H of sulfonated aniline and pyrrole ions is determined to be 0.981 Å. After intercalation of sulfonated aniline and pyrrole ions into the interlayer of MMT, the length of the O–H bond in –SO_3H is calculated to be 1.060 Å and 1.022 Å respectively, which are longer (as shown in Fig. 6). On the basis of the optimized structure, –SO_3H in sulfonated aniline and pyrrole monomers shows distances from surface oxygen atoms on the MMT scaffold of 2.504 Å and 2.593 Å, which are assigned to hydrogen-bonding interactions with relatively high strength.[48] Detailed electronic structure information was used to understand the nature of the elongated O–H bond as shown in Fig. S23;† the deformation charge density between the sulfonated polymer and MMT mainly appears in the (MMT) O···H (sulfonated aniline and pyrrole ions) H-bond, and electron transport occurs more extensively between sulfonated aniline and MMT than between sulfonated pyrrole and MMT, which may explain the stronger acidity of MMT@PAN-[C_3N][SO_3CF_3] found in the experiments. While this preliminary study ignores the heterogeneity of the system, the DFT calculation suggests a plausible mechanism to understand the drastically enhanced acid strength of the 2D solid superacids and is consistent with ^{31}P and ^{1}H solid-state NMR, Hammett indicators and potentiometric titration methods.

Besides the MMT scaffold, graphite oxide can also serve as the layered nanostructure for incorporation of PAN-[C_3N][SO_3CF_3] to give the 2D solid acid GO@PAN-[C_3N][SO_3CF_3]. The product was confirmed from XRD patterns, Raman spectra, electron microscopy and XPS spectra (Fig. S24–S27†). However, no H-bond interaction was observed between PAN-[C_3N][SO_3CF_3] and GO in the synthesized GO@PAN-[C_3N][SO_3CF_3] (Fig. S28†), which may be attributed to the lower oxygen contents and electron-rich network of GO in comparison with the MMT scaffold. As a result, GO@PAN-[C_3N][SO_3CF_3] shows a much weaker acid strength than MMT@PAN-[C_3N][SO_3CF_3] (Fig. S29†). The control over the molecular interactions between acidic sites and the layered scaffolds plays a crucial role in the enhancement of the acid strength of 2D solid acid catalysts.

Conclusions

In summary, a unique type of 2D hybrid solid superacid was developed by incorporating sulfonated polymers in-between MMT layers, with extensive H-bond interactions between MMT and the –SO_3H moiety in polymers. This molecular interaction weakens the O–H bond in –SO_3H, promotes the release of H^+, and thereafter allows for the preparation of solid acids with one of the record high acid strengths. In addition, the 2D layered structures in the solid acids possess a broad distribution of pore sizes and tunable wettability, which promote the mass transportation of molecules into and out of the system and provide

good accessibility of the acidic sites. As a result, the 2D hybrid solid acids show excellent performance for biomass conversion to fuels. This work may provide a new concept for designing solid acid catalysts with both highly efficient mass transport and extremely strong acidity, which may find useful industrial applications in the future.

Conflicts of interest

There are no conflicts to declare.

Acknowledgements

We acknowledge the financial support from the National Natural Science Foundation of China (grant no. 21573150, 21203122, 21522310, 21473244 and 91645112), the Natural Science Foundation of Zhejiang Province (LY15B030002), the Natural Science Foundation of Hubei Province (2018CFA009), the Key Research Program of Frontier Sciences, CAS (No. QYZDB-SSW-SLH026) and the Program for Qishan Scholar of Fuzhou University (GXRC-18043). We thank Prof. Yao Lin at the University of Connecticut for his helpful suggestions and discussions.

Notes and references

1 A. Corma, *Chem. Rev.*, 1997, **97**, 2373–2419.
2 A. Corma, *Chem. Rev.*, 1995, **95**, 559–614.
3 M. E. Davis, *Nature*, 2002, **417**, 813–821.
4 C. Tagusagawa, A. Takagaki, S. Hayashi and K. Domen, *J. Am. Chem. Soc.*, 2008, **130**, 7230–7231.
5 A. Corma and H. García, *Chem. Rev.*, 2003, **103**, 4307–4366.
6 A. Zheng, S. Liu and F. Deng, *Chem. Rev.*, 2007, **117**, 12475–12531.
7 M. Choi, K. Na, J. Kim, Y. Sakamoto, O. Terasaki and R. Ryoo, *Nature*, 2009, **461**, 246–249.
8 S. Suganuma, K. Nakajima, M. Kitano, D. Yamaguchi, H. Kato, S. Hayashi and M. Hara, *J. Am. Chem. Soc.*, 2008, **130**, 12787–12793.
9 A. M. Zheng, S. Li, S. B. Liu and F. Deng, *Acc. Chem. Res.*, 2016, **49**, 655–663.
10 X. Zhang, Y. Zhao and Q. H. Yang, *J. Catal.*, 2014, **320**, 180–188.
11 J. C. Jiang, F. Gándara, Y. B. Zhang, K. Na, O. M. Yaghi and W. G. Klemperer, *J. Am. Chem. Soc.*, 2014, **136**, 12844–12847.
12 M. Hara, T. Yoshida, A. Takagaki, A. Takata, J. N. Kondo, S. Hayashi and K. Domen, *Angew. Chem., Int. Ed.*, 2004, **43**, 2955–2958.
13 K. Inumaru, T. Ishihara, Y. Kamiya, T. Okuhara and S. Yamanaka, *Angew. Chem., Int. Ed.*, 2007, **46**, 7625–7628.
14 P. Barbaro and F. Liguori, *Chem. Rev.*, 2009, **109**, 515–529.
15 E. Nikolla, Y. Román-Leshkov, M. Moliner and M. E. Davis, *ACS Catal.*, 2011, **1**, 408–410.
16 K. Nakajima, Y. Baba, R. Noma, M. Kitano, J. N. Kondo, S. Hayashi and M. Hara, *J. Am. Chem. Soc.*, 2011, **133**, 4224–4227.
17 M. Dusselier, P. V. Wouwe, A. Dewaele, P. A. Jacobs and B. F. Sels, *Science*, 2015, **349**, 78–80.
18 R. Rinaldi, R. Palkovits and F. Schüth, *Angew. Chem., Int. Ed.*, 2008, **47**, 8047–8050.
19 M. Toda, A. Takagaki, M. Okamura, J. N. Kondo, S. Hayashi, K. Domen and M. Hara, *Nature*, 2005, **438**, 178.
20 E. R. Sacia, M. Balakrishnan and A. T. Bell, *J. Catal.*, 2014, **313**, 70–79.
21 F. J. Liu, W. P. Kong, C. Z. Qi, L. F. Zhu and F.-S. Xiao, *ACS Catal.*, 2012, **2**, 565–572.
22 F. J. Liu, L. Wang, Q. Sun, L. F. Zhu, X. J. Meng and F.-S. Xiao, *J. Am. Chem. Soc.*, 2012, **134**, 16948–16950.
23 M. A. Harmer, W. E. Farneth and Q. Sun, *J. Am. Chem. Soc.*, 1996, **118**, 7708–7715.
24 X. M. Zhang, Y. P. Zhao, S. T. Xu, Y. Yang, J. Liu, Y. X. Wei and Q. H. Yang, *Nat. Commun.*, 2014, **5**, 3170.
25 F. J. Liu, J. Sun, L. F. Zhu, X. J. Meng, C. Z. Qi and F.-S. Xiao, *J. Mater. Chem.*, 2012, **22**, 5495–5502.
26 J. Ji, G. Zhang, H. Chen, S. Wang, G. Zhang, F. Zhang and X. Fan, *Chem. Sci.*, 2011, **2**, 484–487.
27 F. Lin, J. Zhang, D. Liu and Y. Chin, *Angew. Chem., Int. Ed.*, 2018, **57**, 12886–12890.
28 D. Deng, K. Novoselov, Q. Fu, N. Zheng, Z. Q. Tian and X. Bao, *Nat. Nanotechnol.*, 2016, **11**, 218–230.
29 C. Tan, X. Gao, X. Wu, Q. He, J. Yang, X. Zhang, J. Chen, W. Zhao, S. Han, G. Nam, M. Sindoro and H. Zhang, *Chem. Rev.*, 2017, **117**, 6225–6331.
30 A. Takagaki, C. Tagusagawa, S. Hayashi, M. Hara and K. Domen, *Energy Environ. Sci.*, 2010, **3**, 82–93.
31 A. Takagaki, M. Sugisawa, D. Lu, J. N. Kondo, M. Hara, K. Domen and S. Hayashi, *J. Am. Chem. Soc.*, 2003, **125**, 5479–5485.
32 X. Zhang, L. Zhang and Q. H. Yang, *J. Mater. Chem. A*, 2014, **2**, 7546–7554.
33 M. Alvaro, A. Corma, D. Das, V. Fornés and H. García, *Chem. Commun.*, 2004, **10**, 956–957.
34 M. C. Laufer, H. Hausmann and W. F. Hölderich, *J. Catal.*, 2003, **218**, 315–320.
35 X. M. Zhang, B. Xiao, J. J. Chen, M. Guo and Q. H. Yang, *Top. Catal.*, 2016, **59**, 1748–1756.
36 C. M. Li, J. Yang, P. Y. Wang, J. Liu and Q. H. Yang, *Microporous Mesoporous Mater.*, 2009, **123**, 228–233.
37 W. Ding, Z. D. Wei, S. Chen, X. Qi, T. Yang, J. Hu, D. Wang, L.-J. Wan, S. F. Alvi and L. Li, *Angew. Chem., Int. Ed.*, 2013, **52**, 11755–11759.
38 K. Chen, M. Abdolrhamani, E. Sheets, J. Freeman, G. Ward and J. White, *J. Am. Chem. Soc.*, 2017, **139**, 18698–18704.
39 C. Trickett, T. Popp, J. Su, C. Yan, J. Weisberg, A. Huq, P. Urban, J. Jiang, M. Kalmutzki, Q. Liu, J. Baek, M. Head-Gordon, G. Somorjai, J. Reimer and O. M. Yaghi, *Nat. Chem.*, 2019, **11**, 170–176.
40 Y. H. Wang, F. Wang, Q. Song, Q. Xin, S. T. Xu and J. Xu, *J. Am. Chem. Soc.*, 2013, **135**, 1506–1515.
41 U. Flessner, D. J. Jones, J. Rozière, J. Zajac, L. Storaro, M. Lenarda, M. Pavan, A. Jiménez-López, E. Rodríguez-Castellón, M. Trombetta and G. Busca, *J. Mol. Catal. A: Chem.*, 2001, **168**, 247–256.

42 J. F. Kögel, A. Y. Timoshkin, A. Schröder, E. Lork and J. Beckmann, *Chem. Sci.*, 2018, **9**, 8178–8183.
43 S. J. Huang, C. Y. Yang, A. M. Zheng, N. D. Feng, N. N. Yu, P.-H. Wu, Y.-C. Chang, Y.-C. Lin, F. Deng and S.-B. Liu, *Chem.–Asian J.*, 2011, **6**, 137–148.
44 W.-H. Chen, H.-H. Ko, A. Sakthivel, S.-J. Huang, S.-H. Liu, A.-Y. Lo, T.-C. Tsai and S.-B. Liu, *Catal. Today*, 2006, **116**, 111–120.
45 M. Kuzminska, T. V. Kovalchuk, R. Backov and E. M. Gaigneaux, *J. Catal.*, 2014, **320**, 1–8.
46 J. Q. Wang, N. Y. Yu, A. M. Zheng, J. Yang, D. Wu, Y. H. Sun, C. H. Ye and F. Deng, *Microporous Mesoporous Mater.*, 2006, **89**, 219–226.
47 S. M. Ma, X. C. Qi, Y. G. Cao, S. G. Yang and J. Xu, *Polymer*, 2013, **54**, 5382–5390.
48 G. A. Jeffrey, *An introduction to hydrogen bonding*, Oxford University Press, New York, 1997.